Process Safety and Environmental Protection 172 (2023) 546–561

Contents lists available at ScienceDirect

Process Safety and Environmental Protection

journal homepage: www.journals.elsevier.com/process-safety-and-environmental-protection

Data-driven modeling of energy-exergy in marine engines by supervised ANNs based on fuel type and injection angle classification

Hadi Taghavifar *, Lokukaluge P. Perera

Department of Technology and Safety, UiT the Arctic University of Norway, Tromsø, Norway

ARTICLE INFO

Keywords:
ANN
Engine modification
Exergy
Homogeneity factor
Hydrogen
Marine diesel engine

ABSTRACT

The application of artificial neural networks with the involvement of a modified homogeneity factor to predict exergetic terms from combustive and/or mixing dynamics in a marine engine is considered in this study. This is a significant step since the mathematical formulation of exergy in combustion is complicated and even unconvincing due to the turbulent and highly nonlinear nature of the combustion process. The computational simulations are carried out on a marine CI (compression ignition) engine and the respective data per different fuel types that are used for thermodynamic exergetic computations as well as energetic simulations. A new parameter namely the modified homogeneity factor derived by an artificial neural network (ANN) is considered for the mixing dynamics, i.e. as an input parameter for the availability and irreversibility predictions. This parameter is based on the standard deviation from an ideal air-fuel mixture formed within the combustion chamber of the marine engine. Furthermore, spray and injection quantities along with the combustion process and its heat transfer parameters are served to predict the exergetic terms for two study cases: (a) fuel type and (b) injection orientation. It is shown that using data analytics that consists of neural networks can provide an adequate approach in diesel engines for improving energy efficiency and reducing emissions.

1. Introduction

New technological advancements in engine and power-generating systems require the employment of an updated approach to solve the energy-emission crisis in the shipping industry (Perera and Mo, 2016). According to new European Union (EU) greenhouse gas (GHG) regulations in the shipping sector, a 55% reduction of total GHG and a full decarbonization mandate is underway by 2050 ambition (DNV, 2018; Liu et al., 2021). The proposed initiatives include the energy taxation directives, where the alternative and promising green fuels are tax-exempt, and the heavy fuel oil is penalized by 37 €/ton (Goulielmos, 2022). This approach can trigger a drastic research campaign to address the alternative fuel applications in internal combustion engines (ICEs) to cope with the emission control and energy management requirements in shipping. Although diesel engines raise concerns over efficiency and emissions, they are still in use in transport and agriculture industries due to their reliability and high power output capabilities (Huang et al., 2022). The recent research studies on diesel engines try to address the shortcomings of such engines to spot energy losses and obviate emissions.

Machine learning and big-data analyses in maritime have proved enormous capacity to handle large-scale data sets, i.e., both in clustering/classification and trend recognition/regression (Perera et al., 2016) and behavior prediction of vessels and ship systems (Castresana et al., 2022a). In this setting, artificial intelligence techniques and soft-computing methods streamline fast predictive models of marine engine performance without resorting to unwieldy experimental approaches and hefty numerical simulations producing instant online responses even for the unseen input data with a higher degree of confidence (Maind and Wankar, 2014; Taghavifar et al., 2016, 2014). Artificial neural network (ANN) based models can be utilized in terms of dealing with non-linear problems, where the physical connection that exists between input-output parameters may not be straightforward (Niu et al., 2017). However, ANN approaches should relate to the combustion process of IC engines through the principles of thermodynamics to model such conditions.

The second law of thermodynamics, which governs the energy accessibility and convertibility of energy-to-work ratio potential, can support the energy analysis of marine engines (Dincer and Rosen, 2012). It is an insightful approach to efficiency analysis to address the energy

* Corresponding author.
E-mail address: hadi.taghavifar@uit.no (H. Taghavifar).

https://doi.org/10.1016/j.psep.2023.02.034
Received 18 July 2022; Received in revised form 24 November 2022; Accepted 13 February 2023
Available online 16 February 2023

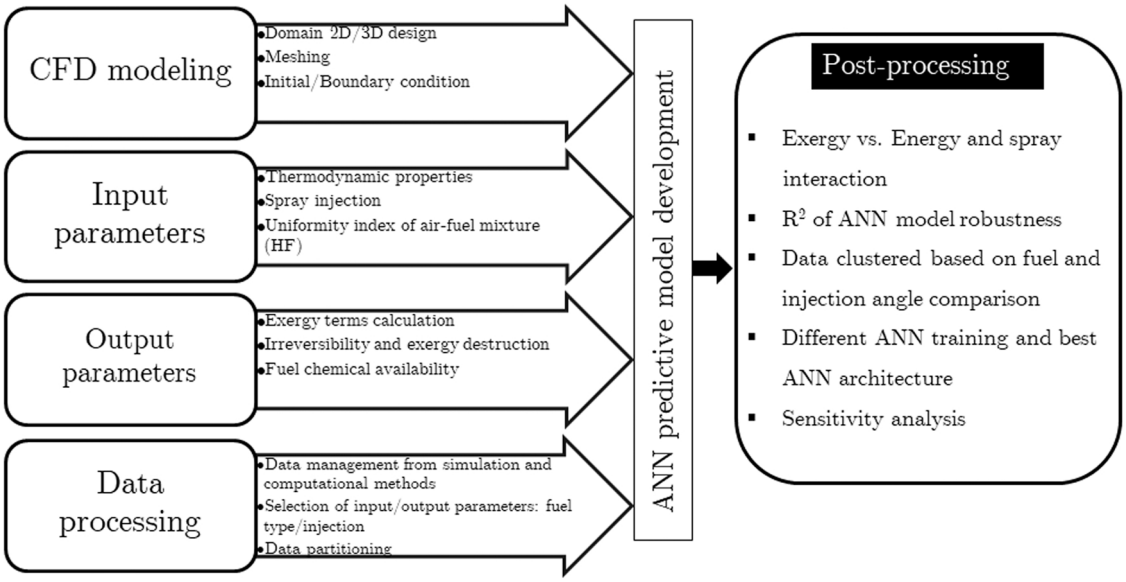

Fig. 1. The research pathway: step-by-step flow diagram.

quality in each system. The entropy creation in a process dissipates the chances of energy utilization and increases the non-ideality or irreversibility that translates to the degradation of energy systems (Demirel, 2007).

Various fuel types can be used to create thermal energy through the combustion process of engines. Dimethyl ether (DME) is a clean colorless gas with non-toxic properties, which can be liquefied and injected in the engine to obtain zero particulate and sulfur emissions (Makoś et al., 2019). This fuel can be an acceptable alternative fuel for marine powertrains and ship propulsion system with affordable retrofitting and infrastructure launching (competitive costing around 523 $/t to 604 $/t) (ChemBioPower, 2019). Hydrogen as fuel in the ship powertrain is another option that can partially (and in rare cases even fully) replace diesel or heavy fuel oil (HFO) to eliminate SOx and GHGs, although the concerns over its transportability, storage, production, and safety can be considered as challenges.

In another relevant study, the objective is set on an ANN coupling with a non-dominating sorting genetic algorithm (NSGA-II). The intelligent data handling approach is implemented on a dual-fuel, low-temperature combustion engine to increase the exergy efficiency and decrease the exergy destruction (Shirvani et al., 2021). This research has utilized an optimization technique to vary the input data of the simulated engine so that the objective function of an optimization algorithm be satisfied. As reported, the best candidate solution managed the NOx and soot amount to satisfy the emission control regulations. Iscan (Işcan, 2020) has used ANNs on the experimental results of a diesel engine running with safflower biodiesel to explore the thermodynamic elements of the combustion system. The combustion parameters served as the inputs such as burned fuel mass fraction, heat transfer velocity, and heat release rate (HRR) sorted with respect to the engine load. The author claimed that the ANN has a higher capability in predicting the engine performance (e.g., brake thermal efficiency) and emission metrics (e.g., NOx and CO2) for both diesel and biodiesel fuels. Can et al (Can et al., 2022). considered ANN as a predictive data-processing tool to generate the output results of a diesel engine. The study argued that the developed network can learn the trend between input-out results with a correlation coefficient of R = 0.999 that satisfies a low error criterion. As discussed, the results show that the ANN can be a potential option for combustion diagnostic/control as virtual sensors and engine calibration methodologies. Ma et al (Ma et al., 2022). used ANN and particle swarm optimization (PSO) algorithm to establish a predictive model and to optimize the dual-fuel marine engine performance and emission. They reported the fuel consumption (2.1% declined brake specific fuel consumption (BSFC)) and emission reduction (20.5% NOx & 43.1% CO) accomplishment as the optimization target by tuning the respective operational variables. Raptodimos and Lazakis (Raptodimos and Lazakis, 2020) used a Nonlinear Autoregressive technique with an Exogenous Input (NARX) neural network to assess its prediction feasibility of the marine engine performance index (the exhaust gas temperature of a marine main engine). Their results indicate that the network can predict the exhaust gas temperature of the ship engine and thereby sends a warning signal for future anomaly in the engine operation. Besides the predictability characteristics of artificial intelligence (AI) and machine learning techniques in marine engine applications, the respective functions are based on data clustering (Raptodimos and Lazakis, 2018; Bui and Perera, 2021) and fault diagnosis (Zhou and Xu, 2010; Xu et al., 2017) techniques.

From the literature, the studies revolving around engine exergy forecasting via AI and in specific ANN are scarce. Most of the investigated works attempt to predict the engine outperformance and emission elements based on the selective input variables, such as load, pressure, temperature, etc. These input and output variables can be matched by training neural networks. This study bridged the gap between the first law (energy conservation) and the second law (exergy) of thermodynamics through neural network modeling where various spray and mixing mechanics factors are involved that have not been captured in mathematical models. In order to further emphasize the validity of responses, the simulated and computed data are generated and classified into two classes: case study 1 (sorted based on fuel types) and case study 2 (sorted based on spray injection angle). The availability and irreversibility as the second law thermodynamic analysis components are linked to spray-combustion-emission as the input whereas these parameters are recognized mostly as the output in former research outlets. The main contribution of this study is on the methodology, novel input/output quantities selection, modularity, and adaptability of the neural network with alternative-renewable fuels and new operational spray injection angle. The authors believe that premixing and post-mixture quality is the underlying parameter in both energy efficiency and exergy output of the marine engine. As a result, instead of the air-fuel equivalence ratio, the modified homogeneity factor for different fuels and injection angles is calculated and then included in the input layer of the network. The interconnection of far initial (spray and mixing) and far post-combustion (exergy) parameter arranged as the inputs-outputs in the network platform with successful forecasting accuracy is the

Table 1
Engine characteristics and applied simulation models.

Parameter	Value/comment
Bore × stroke	160 × 240 (mm^2)
Cylinder number/engine layout	6/ in-line
Rated speed/power	1000 rpm/540 kW
Compression ratio	15.2
Fluid flow field turbulence model	*k-ζ-f* (Popovac and Hanjalic, 2007)
Spray-wall collision	Walljet 1 (Cabrera, 2003)
Conservative equations discretization algorithm	Simple/Piso (Versteeg and Malalasekera, 2007)
Combustion model	Coherent flame model: ECFM-3Z+ (Colin and Benkenida, 2004)
Spray evaporation	Duckowicz (Dukowicz, 1980)
NOx model	Extended Zeldovich (Zeldovich et al., 1947)

advancing step of the present study by the combination of CFD, thermodynamic analysis, and big-data machine learning applications.

The undertaken steps from data generation and sorting to ANN modeling and post-processing are demonstrated in Fig. 1 to better illustrate and summarize the research targets.

2. Marine engine specification

The engine considered for the data analysis is a marine medium-speed, four-stroke with six-cylinders unit and that the key features are listed in Table 1 (Hu et al., 2017). Since the purpose of this research is to focus on data-driven modeling of the energy-exergy correlation, the main simulation models are also listed in Table 1, which led to a valid engine output result.

The computational simulations are performed via the AVL-FIRE platform (AVL FIRE version, 2018) where the structural dimensions of the chamber, crankshaft, connecting rod, injection line, and valves are taken from the experimentally operated engine. The meshed domain of the combustion chamber in two topologies of top dead center (TDC) (720 °CA) and 730 °CA are displayed in Fig. 2. The local grid refinement in the spray block is implemented from 40 CA bTDC (before top dead center) to 40 CA aTDC (after top dead center) to upgrade the precision of spray injection and droplet evaporation. The average cell size is 0.7 mm, hence the cell number generated in this method is 103616. The transient modeling of different 4 strokes of engine operation is implemented by crank-angle (CA) run mode where the CA intervals are split into different steps with smaller ones at initialization of 0.1 CA and fuel injection and combustion period of 0.2 crank-angle, whereas for the compression 2 CA step is considered to speed up the running time. The initial condition quantities of turbulent kinetic energy, turbulent length scale, and turbulent dissipation rate are adjusted to 10 m^2/s^2, 0.001 m, and 5231 m^2/s^3.

3. Exergy terms and modified homogeneity factor (HF*) calculations

The data acquired for the neural network in the next stage of the study are categorized as either direct parameters (calculated as the energy quantities taken from the CFD solution) or have to be further evaluated in an indirect format. The following parameters are the indirect parameters that are computed analytically or by the EES (engineering equation solver) tool.

3.1. Exergy expressions in the output of the network

The exergy/availability is defined as the quantity related to a dual system-environment interaction where the system is brought to the dead-state equilibrium condition of the surrounding, thus producing useful/convertible work (Moran et al., 2010). The exergy stems from the second law of thermodynamics that argues over the quality of energy rather than the amount of energy. As a result, this study is dealing with the quality of the energy delivered from the engine system and detects the sources of energy loss and the irreversibility that undermines the ratio of the transmittable energy and work. The irreversibility in this

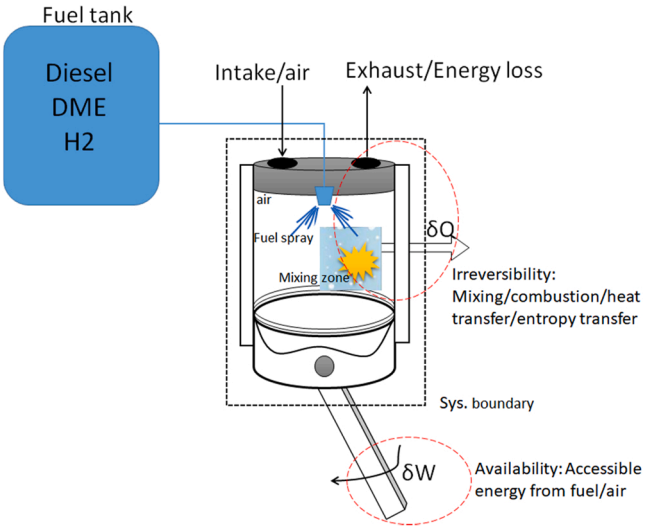

Fig. 3. Schematic representation of irreversibility and availability in the system boundary of cylinder-piston arrangement.

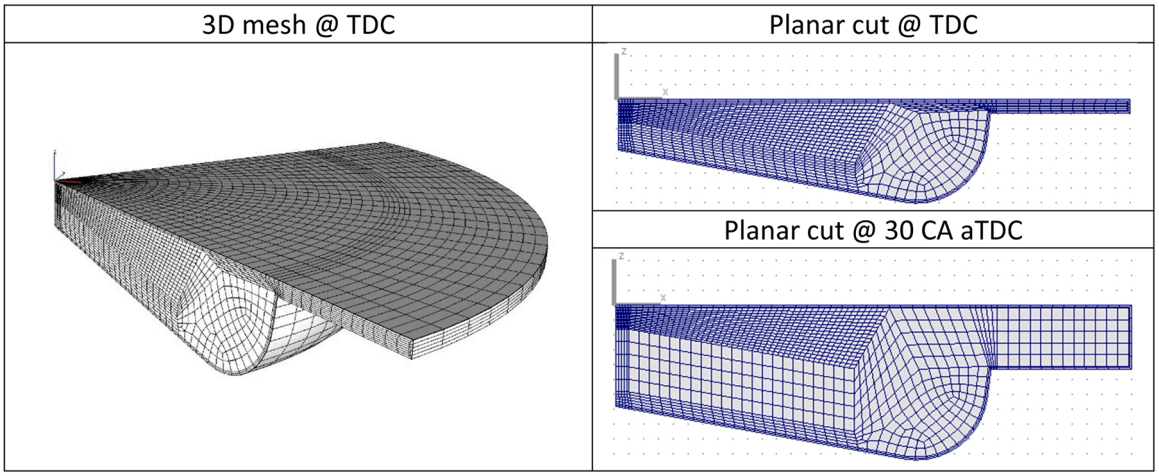

Fig. 2. The meshed domain of combustion chamber at different CA positions.

research not only comes from the combustion, and heat transfer processes but also the air-fuel mixing process contributes to the irreversibility process (Terzi, 2018). The total availability constitutes chemical and thermomechanical components of the in-cylinder phenomena. A schematic of the energy/exergy balance on the combustion chamber as the system boundary is depicted in Fig. 3. The provided energy of fuels' chemical energy released by the oxidation process within the cylinder chamber produces heat and pressure. The heat is transferred via the cylinder walls or transported as gas mass flow from the outlet exhaust valve. The heat portion of the generated energy in the combustion chamber is inaccessible and results in the process irreversibility. However, the generated pressure in cylinder can contribute to useful work that propels the system hence increasing the exergy of the engine as illustrated in Fig. 3. The sprayed fuel mixing with air, combustion process, energy transport as enthalpy from the exhaust valves, and the heat transfer due to a definite temperature difference between the cylinder wall and the ambient air are main sources of the irreversibility that tend to undermine the availability of the supplied energy in the combustion chamber of the engine as identified in the following schematic representation.

The chemical and thermomechanical availabilities (A_{ch} and A_{tm}) are estimated as follows, having thermodynamic properties and mass flow across the system boundary (Van Gerpen and Shapiro, 1990):

$$A_{ch} = T_0 \sum_i m_i R_i \ln\left(\frac{x_i}{x_i^0}\right) \tag{1}$$

$$A_{tm} = E - P_0 V - T_0 S - \sum_{i=1}^{kk} \mu_{i0} m_i \tag{2}$$

where P_0 and T_0 represent the equilibrium dead-state conditions pressure and temperature and x_i, μ_i, and m_i give the molar fraction, chemical potential, and mass fraction of species i in the combustion chamber. Therefore, the total energy with the addition of two components can be obtained:

$$A_{tot} = A_{ch} + A_{tm} = E - P_0 V - T_0 S - \sum_{i=1}^{kk} \mu_i{}^0 m_i \tag{3}$$

A_{tot} is the overall availability, while E, V, and S denote the total energy, cylinder volume, and entropy. The irreversibility rate which is associated with exergy destruction is introduces in below equation, therein the exergy destruction is linked to combustion process per CA:

$$\frac{dI}{d\theta} = \frac{T_0}{T} \sum_{i=1}^{kk} \mu_i \frac{dm_i}{d\theta} \tag{4}$$

where $\mu_i = g_i$ is valid for the ideal gases and for fuels $\mu_i = a_{f,ch}$ can be applied. dm/dθ is the mass flow rate with crank-angle and $A_{f,ch}$ is the chemical exergy of fuel with $C_xH_yO_z$ structure is calculated as below (Rakopoulos et al., 2008).

$$A_{f,ch} = m_f a_{f,ch} = LHV\left[1.0410 + 0.01728\frac{x}{y} + 0.0432\frac{z}{y}\right] \tag{5}$$

Where m_f and $a_{f,ch}$ are the fuel mass flow and specific chemical exergy of the fuel, respectively.

3.2. Modified homogeneity factor as mixing mechanics indicator in the input of the network

The mixing process of air/fuel in the combustion chamber is an underlying phase that affects the subsequent combustion and ignition timing. This, in return, alters the kinetics of the chemical reaction. The mixing process eventually impacts the generated species during the combustion, the concentration of species, and burning rate. Therefore, the measurement of mixing quality and extent of the uniformity is proposed based on a new definition of the heterogeneity factor (Nandha and Abraham, 2002) and then the improved coefficient of the modified homogeneity factor (HF*) is introduced (Taghavifar et al., 2021).

In the former definition, the mixture heterogeneity can be described as the standard deviation of the dimensionless fuel mass by the total mixture mass. In this manner, the distribution of fuel in each computational cell must be considered, thereby the increase of fuel in each cell (cell i) means that the fuel amount in the adjacent cell will be decreased. Hence, the half of fuel standard deviation is the criteria for the computations of fuel dispersion in the combustion chamber domain. The change in the fuel amount in the *i-th* cell depends on the average equivalence ratio (φ_0) as (Mobasheri and Peng, 2013):

$$dm_f = \frac{\varphi_i}{AFR_{st} + \varphi_i}\delta m_i \quad dm_a = \frac{AFR_{st}}{AFR_{st} + \varphi_i}\delta m_i \rightarrow \left(dm_f\right)_{cell\ i} - \left(\overline{dm}_f\right) = \frac{\varphi_i}{AFR_{st}}\delta m_i - \frac{\varphi_0}{AFR_{st}+}\delta m_i$$
$$\rightarrow = \frac{AFR_{st}(\varphi_i - \varphi_0)}{(AFR_{st} + \varphi_i)(AFR_{st} + \varphi_0)}\delta m_i \tag{6}$$

In the new definition, instead of the fuel mass, the optimal mixture of air/fuel mass and its deviation from the mean value of the ideal mixture is adopted and then scaled as a non-dimensional coefficient. Eq. 6 in a simple format gives the fuel mass variation in a given computational cell based on the equivalence ratio and AFR_{st}. The optimal mixture takes the independent constants of air and fuel in the cell. The assigned coefficients of fuel and air are multiplied by the mass fraction of air and fuel in each respective mass fraction and then summed over (Taghavifar et al., 2021):

$$L_i = A(dm_a)_i + B\left(dm_f\right)_i$$
$$L_i = x(dm_a)_i + AFR_{st}\left(dm_f\right)_i = \left[\frac{xAFR_{st}}{AFR_{st}+\varphi_i} + \frac{\varphi_i AFR_{st}}{AFR_{st}+\varphi_i}\right]\delta m_i = \frac{(x+\varphi_i)AFR_{st}}{AFR_{st}+\varphi_i}\delta m_i \tag{7}$$

here φ_i represents the equivalence ratio at cell i, dm_a and dm_f are the mass fractions of air and fuel. The coefficients are $A = x$ and $B = AFR_{st}$ where x such varies that the standard deviation from the ideal non-dimensional mixture results the minimum of *HeterF(θ)* or alternatively maximum of *HF** as:

$$HeterF(\theta) = \frac{\sqrt{\sum_{i=0}^{N_{cell}} \left[(L - \overline{L})_i\right]^2}}{2\overline{L}}$$
$$HF^*(\theta) = (1 - Heter\ F(\theta))\ \% \tag{8}$$

The HeterF(θ) function shows non-uniformity of the air-fuel mixture and is the opposite of homogeneity factor (HF*).

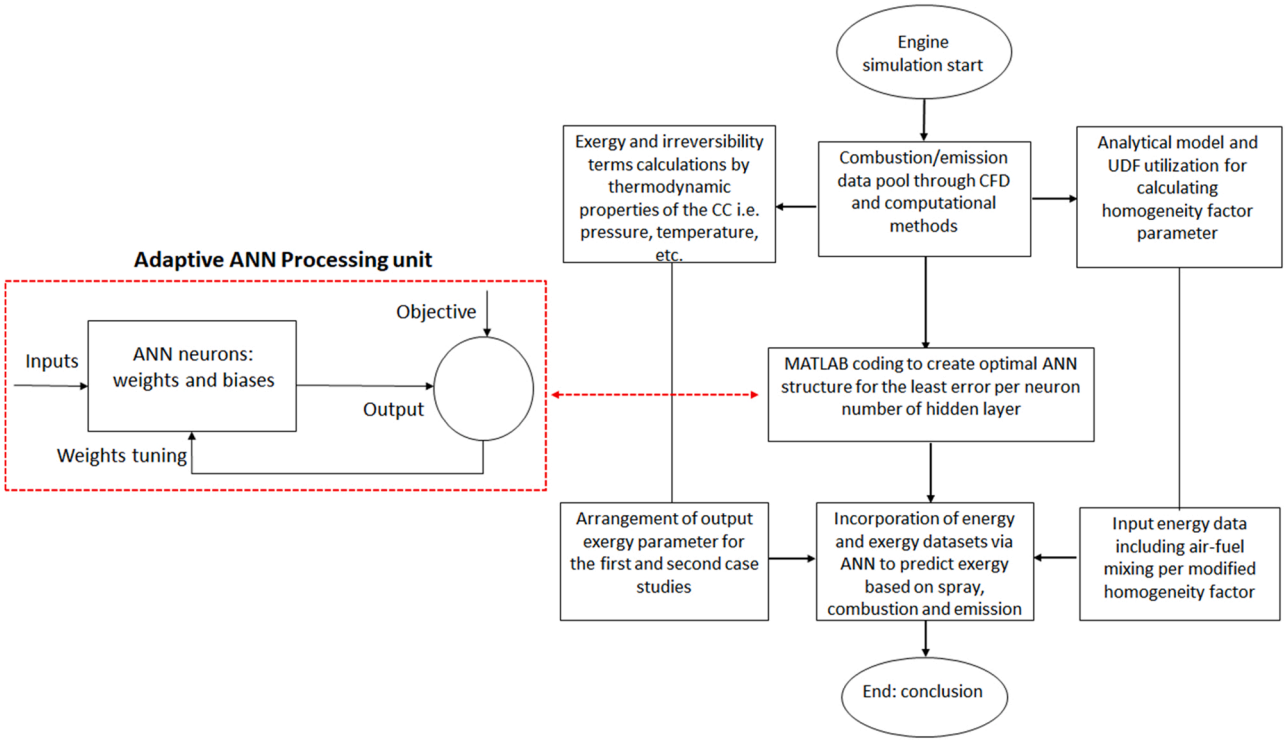

Fig. 4. Energy-exergy thermodynamic dataset acquirement and handling with supervised ANN network predictive model.

4. Implementation of ANN on energy-exergy datasets

The ANN framework is categorized among utilitarian soft-computing knowledge and artificial intelligence perspective. This science has gained widespread popularity within pure and applied science areas. This modeling domain is a dynamic research field for scientists, where ANN has proved efficiency potency in facing complex nonlinear systems. The ANN mimics the human biological behavior of a neuron system where each neuron is composed of weights and associated biases that are connected through multiple convoluted layers. The number of layers is determined based on the complexity of the problem. These networks are called multi-layer perceptron (MLP) networks with hidden layers between input and output that have a characteristic role in the predictive capacity of the developed ANN. The input layer of the network takes the input parameters as the input neurons and process them through the hidden layers and gives out output parameters in the output layer. These networks are featured as modular and adaptable with various structures. Once the inputs are fed to the network and a specified amount is presented as an objective, the error can be obtained via a comparison of desirable and actual responses of the system. The acquired error then will be back-propagated to the system so that the respective adjustments are administered under the supervised rules of the network. This process will be iterated consecutively until the output reaches a desired and acceptable amount, where the respective error is minimized. The back-propagation algorithm runs until the convergence of the predicted values towards the actual values that are implementable and optimizable through the descent gradient method. The schematic coordination representation of ANN along with input/output parameters and the single hidden layer is demonstrated in Fig. 4.

4.1. Data handling and processing: normalization, classification, and error estimation

A total dataset size of 9760 is used for the modeling with the partitioning of 70%, 20%, and 10% portions randomly allocated for training, testing, and cross-validation, respectively. The Levenberg-Marquardt training algorithm (trainlm) is applied during the modeling implementation due to its acceptability and capability concerning the combustion phenomena in direct injection (DI) engines (Roy et al., 2014). A feed-forward ANN with a back-propagation training algorithm is employed while four training algorithms (trainlm, traingdx, trainmp, and trainscg) are adopted in which the error minimization has been performed by the gradient descent. In the present study, the MLP network prognosticates the responses consisting of one hidden layer with varying neurons of 1–20 which is to avoid random selection in the network structure. During the initial training phase of the network, the weights and biases of the neurons are selected arbitrarily. Therefore, for each number of neurons in the hidden layer (for any given network architecture), the network is trained for 100 iterations to overcome the haphazard selection deficiency. In each training iteration, the network is trained for 1000 epochs. The mean value is considered an efficiency index of the predictive potential of the respective model. Ultimately, in the non-dimensioning step, the following function will be served for the calculation:

$$X_n = \frac{X_r - X_{r,\,\min}}{X_{r,\,\max} - X_{r,\,\min}} \times \left(X_h - X_l\right) + X_l \tag{9}$$

Where X_n denotes non-dimensional input variables, X_r denotes initial unprocessed input variables, and $X_{r,min}$ and $X_{r,max}$ are the minimum and maximum of the input variables. Furthermore, X_h and X_l are 0 and 1 successively. Since the values are placed between 0 and 1, in accordance with dimensionless output, the logsig transfer function is taken. For modeling, the network efficiency is assessed with different statistical indices. The root mean square error (RMSE), mean absolute percentage error (MAPE), and coefficient of determination (R^2) are considered for estimating the predictive quality in the ANN.

$$MAPE = \frac{1}{n}\sum_{i=1}^{n}\left|\frac{Y_{actual} - Y_{predicted}}{Y_{actual}}\right| \tag{10}$$

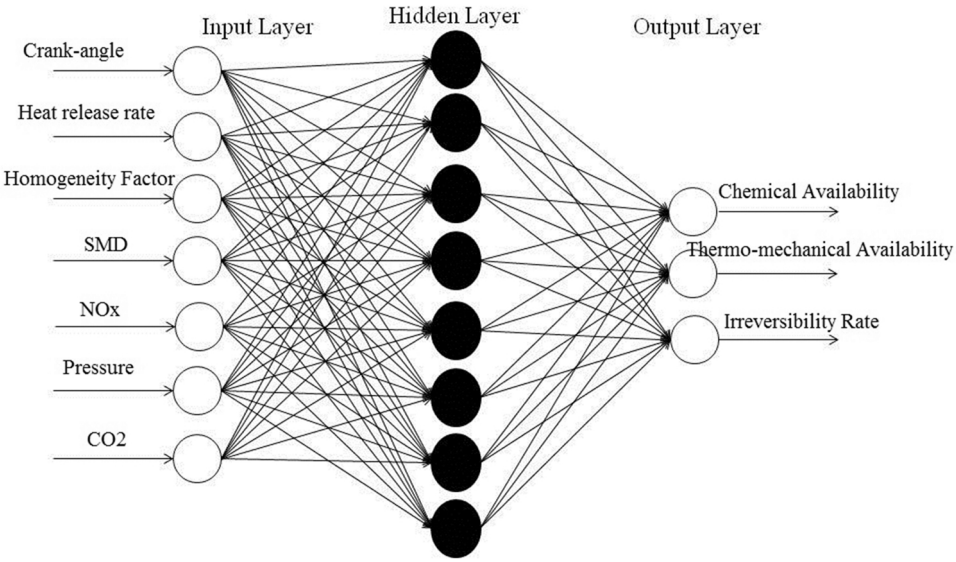

Fig. 5. Block structure of developed ANN for the first case study: fuel type parameter sets.

Table 2
Statistical data of input and output parameters including uncertainty, standard deviation, and variation bounds.

No.	*Objective input and output parameters	Design parameters	Min. and Max. data discrepancy	Std. deviation	%Uncertainty
1	Crank angle (θ)	CA	690–781	20.7	4.6
2	Heat release rate (J/deg)	HRR	0–38.32	10.45	3.296
3	Homogeneity factor (%)	HF	0–0.834	0.321	0.573
4	Sauter mean diameter (mm)	SMD	0–0.143	0.0256	0.1578
5	Nitrogen oxide mass fraction (-)	NOx	0–0.00235	0.000695	0.029
6	Pressure (MPa)	P	1.85–19.8	3.4563	1.983
7	Carbon dioxide mass fraction (-)	CO2	0–0.16073	0.0593	0.232
8	Chemical availability (J)	Ach	0.7983–27.21	8.73909	3.17231
9	Thermo-mechanical Availability (J)	Atm	55.35–635	171.8472	12.9395
10	Irreversibility rate (J/deg)	dI/dθ	0–15.06	4.4627	2.2835

$$RMSE = \sqrt{\frac{1}{n}\sum_{i=1}^{n}\left(Y_{predicted} - Y_{actual}\right)^2} \tag{11}$$

$$R^2 = \frac{\sum_{i=1}^{n}\left(Y_{predicted} - Y_{mean}\right)^2}{\sum_{i=1}^{n}\left(Y_{actual} - Y_{mean}\right)^2} \tag{12}$$

where Y_{actual} و $Y_{predicted}$ are actual and predicted output values calculated by the ANN.

4.2. The ANN architecture configuration and performance analysis

The predictive strength of the network is significantly dependent on its structure. The ANN has essentially comprised of the input and output layers with one or several hidden layers. The principal components of the network include neurons, i.e. transfer functions with predefined layers. The fundamental transfer functions that are used in the MLP layers of the network include Log-Sigmoid (logsig), Tan-Sigmoid (tansig), and linear functions of Purelin. The transfer functions in the neural network can be linear and nonlinear therein a nonlinear function ensures appropriate functioning of the developed ANN within nonlinear system behavior. The network output reliance on the transfer function type must be reiterated. The Logsig function receives the input signals in the range of (-∞, +∞) and converts them into the (0, +1) band.The tansig has data within (-∞, +∞) and transfers the corresponding data into (−1, +1), while Purelin function, also known as linear or identical function, maps (-∞, +∞) data interval into the same domain of (-∞, +∞). In recent research studies, activation functions of Purelin and tansig are adopted for the output and hidden layers respectively since they had demonstrated acceptable performance in the combustion and species gas modeling applications (Paul et al., 2018). The u argument transfer from the input signal region to y output takes place as:

$$y^k = \tan sig\left(u^k\right) \tag{13}$$

The overview of various training algorithm types that have been recently updated and employed in the engineering scope reveals that following are the most efficient (Hoang et al., 2021): (a) resilient backpropagation, (b) scaled conjugate gradient (scg), (c) Levenburg-Marquardt, (d) gradient descent with momentum and adaptive learning (gdx) that for this project, different methods are taken altogether.

5. Results and discussion

The results fall into two major categories of fuel type and injection angle. Each category then is divided into two subcategories: firstly, the network setup and input/output interactions will be addressed, and secondly the obtained results from ANN forecasting will be shown and discussed.

5.1. ANN application on the energy-exergy link with HF* consideration: the first case study- grading based on the fuel type

In the first case study, after much inspection of the factors that can have the highest impact on the elements and components governing the

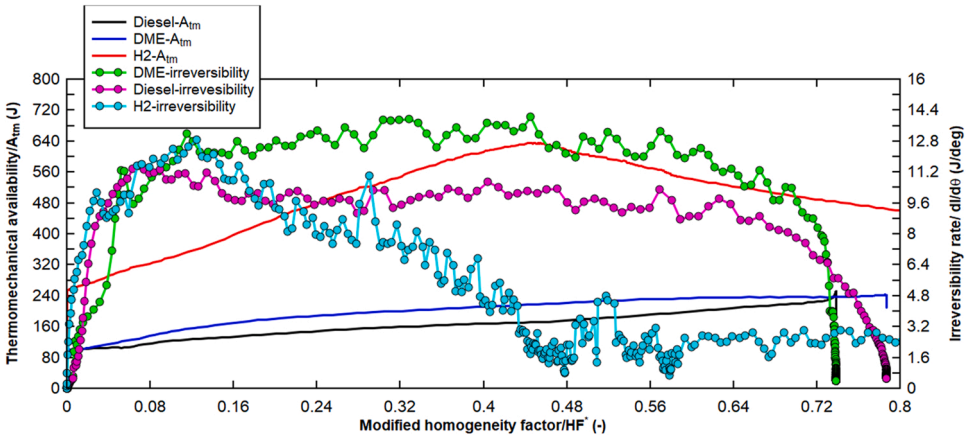

Fig. 6. Thermomechanical and irreversibility rate variations versus HF* for diesel, DME, and hydrogen fuels.

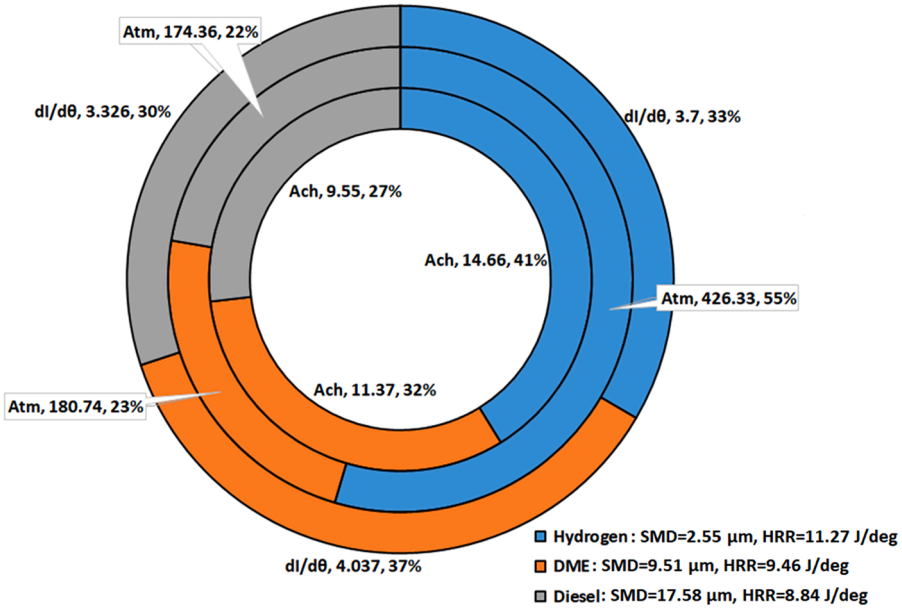

Fig. 7. Pie chart breakdown of chemical/thermomechanical availability and irreversibility rate for diesel, DME, and hydrogen fuels.

second law of thermodynamics (exergy and irreversibility), the crank angle, the rate of heat release rate, the modified homogeneity factor of air/fuel mixture, Sauter mean diameter (SMD) of spray, NOx mass fraction, CO2 mass fraction, and in-cylinder pressure are selected as the influential input variables or parameters on the evolving trend of the exergetic output parameters. The utilized output parameters include chemical availability, mechanical availability, and irreversibility rate. In order to demonstrate the input parameters' effect on the availability in the engine , the broken-down exergy into the chemical and physical (mechanical) availability is used instead of the overall parameter. The classic thermodynamic equations have linked the exergy to the combined factors of the system-environment, such as temperature, pressure, and generated species concentrations (Bejan, 2016). However, in current research, the preceding events of combustion (spray and air/fuel mixing quality), and indirect combustive events (such as heat release rate) are included to increase the precision of the developed model. The schematic representation of the block structure of the network along with neurons and layers is shown in Fig. 5, where the involved input and output parameters can be seen.

The proposed network with the respective number of neurons in the hidden layer can be categorized as: the ANN structure will be 7-x-3 that x represents the number of neurons in the hidden layer. The x value for different training algorithms can be varied and thereby the chosen number is based on the network performance in an organized manner, while in other studies that are mostly chosen based on trial and error, which greatly undermines the efficiency of the developed neural network system. The initial and unprocessed input and output data must be dimensionless within (−1, 1) domain due to the use of the tansig transfer function. This is advantageous since promotes the training feature of the network and prevents the lingering trend and sticking the output results in the local optima. During the start of the network training, the weights and biases are inevitably selected randomly. Therefore, for each number of neurons in the hidden layer, the network is trained100 times to overcome this issue. In general, the network is trained for 1000 epochs as the cutoff parameter to complete its convergence to the respective parameter during the training algorithm.

5.1.1. The relation between inputs and outputs- the first case

The collected data from the selected marine engine is sorted based on CA evolution. Some data are directly from the simulated engine and some of them are further calculated (e.g., modified HF* and exergetic terms). The statistical information is detailed in Table 2, with the list of input-output parameters and the respective numeric significance. With reference to Table 2, it is stated that the highest data sensitivity is

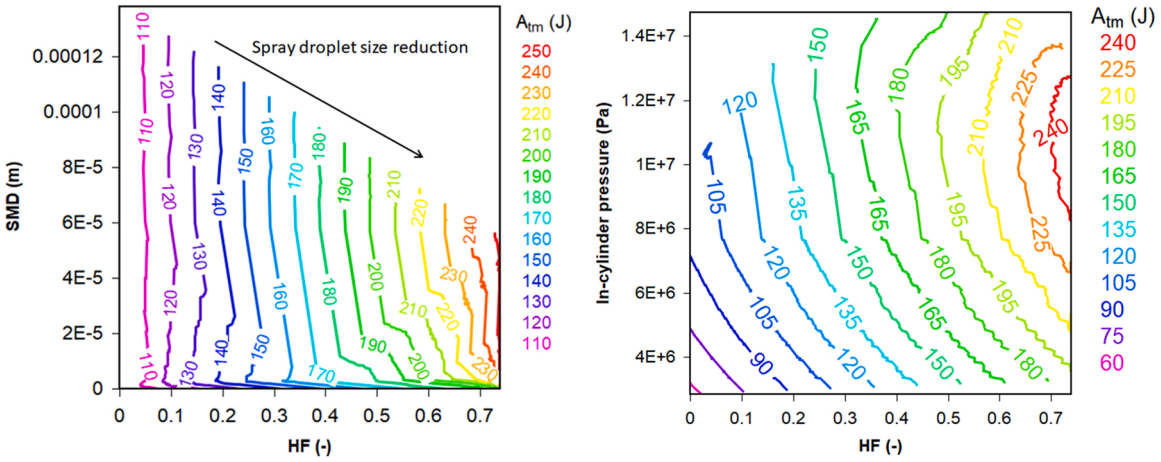

Fig. 8. The impact of input variables of HF, SMD, and pressure on A_{tm}.

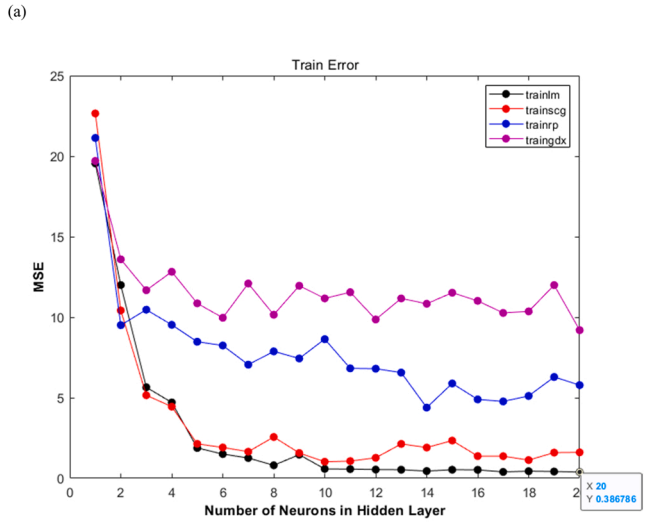

Fig. 9. (a) The MSE variation per neuron number of hidden layer for different training algorithms, (b) magnified view of MSE changes in the 10–20 neurons for trainlm.

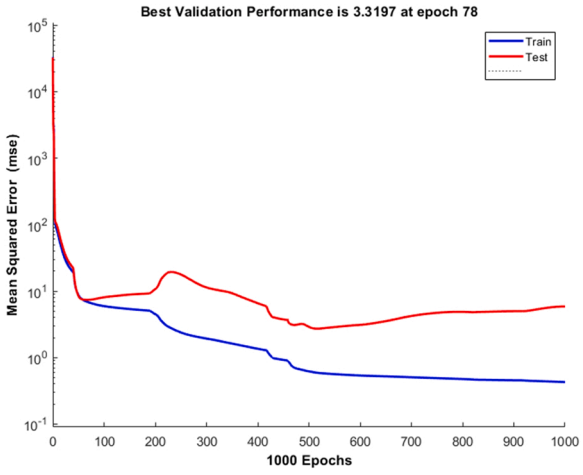

Fig. 10. The MSE variation with the number of iterations as epochs to determine the best validation point for the testing and training phases.

Table 3
Performance and accuracy of the developed ANN for the output parameters for the first case study sets.

Output parameters	R^2		RMSE		MAPE	
	Test	Train	Test	Train	Test	Train
A_{ch}	0.999	0.9999	0.23789	0.20841	0.06259	0.04921
A_{tm}	0.996	1	0.98736	0.76549	0.01943	0.00279
dI/dθ	0.978	0.983	0.60766	0.53758	0.284	0.45034

associated with thermomechanical availability (A_{tm}) and the lowest sensitivity and data discrepancy pertains to the NOx mass fraction.

For better characterization of the significance of HF* on the outlet results, this study deals with this valuable parameter and analyze the findings. To this end, Fig. 6 provides where the variations of the thermomechanical and irreversibility rate with respect to the modified homogeneity factor is plotted for diesel, DME, and hydrogen fuel types. It is seen that as expected with the combustion process of hydrogen correspondingly more availability is achieved compared to other fuels. However, the important point is that hydrogen, unlike the other two fuels, has a peak point with HF* that occurs at HF* = 0.453 while the peak point of diesel and DME are consistently increasing. That is to say, the higher HF* coefficient (that means better air/fuel mixing quality), the system potential or preparatory measures to use the available

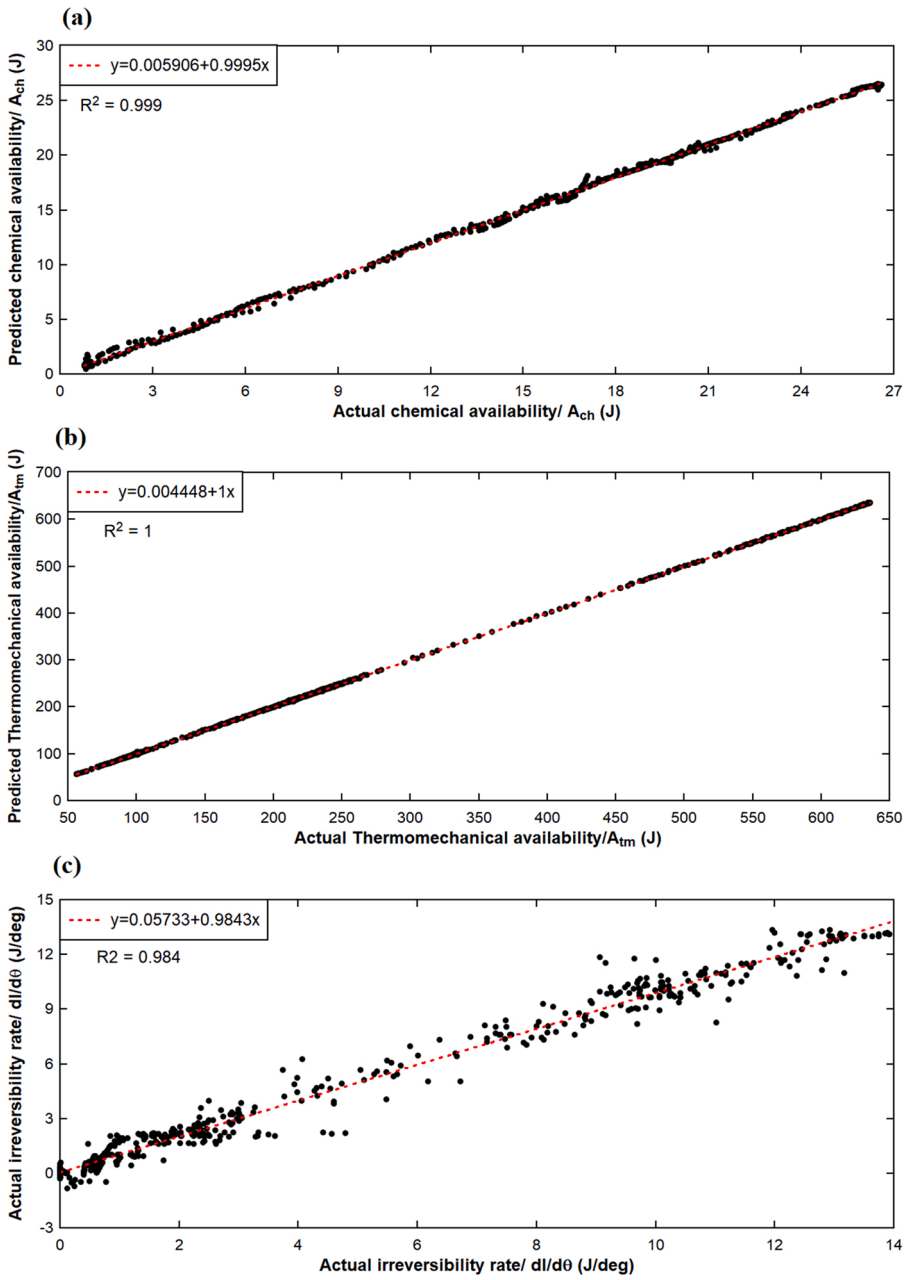

Fig. 11. Scatter plots of comparison between the ANN-predicted and actual output results for (a) A_{ch}, (b) A_{tm}, (c) dI/dθ.

energy, and the energy-to-work chance increases accordingly. Once the mixing quality enhances, better combustion efficiency takes place, hence the chemical reaction releases much more energy. Subsequently, the in-cylinder pressure and temperature rise, and the availability elevate. In the case of hydrogen fuel, it seems that an optimal amount of homogeneity factor leads to maximum thermos-mechanical availability that corresponds to $A_{tm} = 633.8$ J. The optimality point determination depends on the under-investigated engine system characteristics to have enough capacity to use the released energy by fuel with a high heating value to convert the most of chemical energy into the power output. The irreversibility rate curve is strongly oscillatory since the instantaneous irreversibility is calculated at each moment per crank angle that originates from the turbulent nature of the combustion process and severe change of thermodynamic properties. The reason for the higher average irreversibility of DME compared to diesel is attributed to the combustion chamber containing gas entropy and more heat transfer of DME-powered engines to the environment compared to diesel. This mainly stems from high pressure and high-temperature combustion of DME that has been mentioned earlier (Roh and Lee, 2017) and greater average heat release and out heat flux for DME ($HRR_{DME} = 9.46$ J/deg, $HRR_{diesel} = 8.84$, $WHF_{diesel} = 17{,}614$ W, $WHF_{DME} = 21{,}112$ W). Hydrogen exhibits a different trend because after the peak point corresponding to $HF^* = 0.13$, the average irreversibility begins to decline and in a broader view, hydrogen at a higher HF ratio gives much lesser irreversibility than the other two fuels.

Fig. 7 presents the pie chart breakdown of the output parameters for each of the considered fuels with associated properties such as HRR and SMD where the allocated portion for each fuel is separated in percentages. From Fig. 7 it can be interpreted that diesel fuel has a bigger spray droplet diameter SMD = 17.58 μm and a corresponding heat release capability that is the lowest HRR = 8.83 J/deg. This causes it to have the lowest exergy or chemical and thermomechanical availability for this fuel with 27% and 22% share of the total availability, respectively. One can conclude that the fuels with the lower capability to be disintegrated

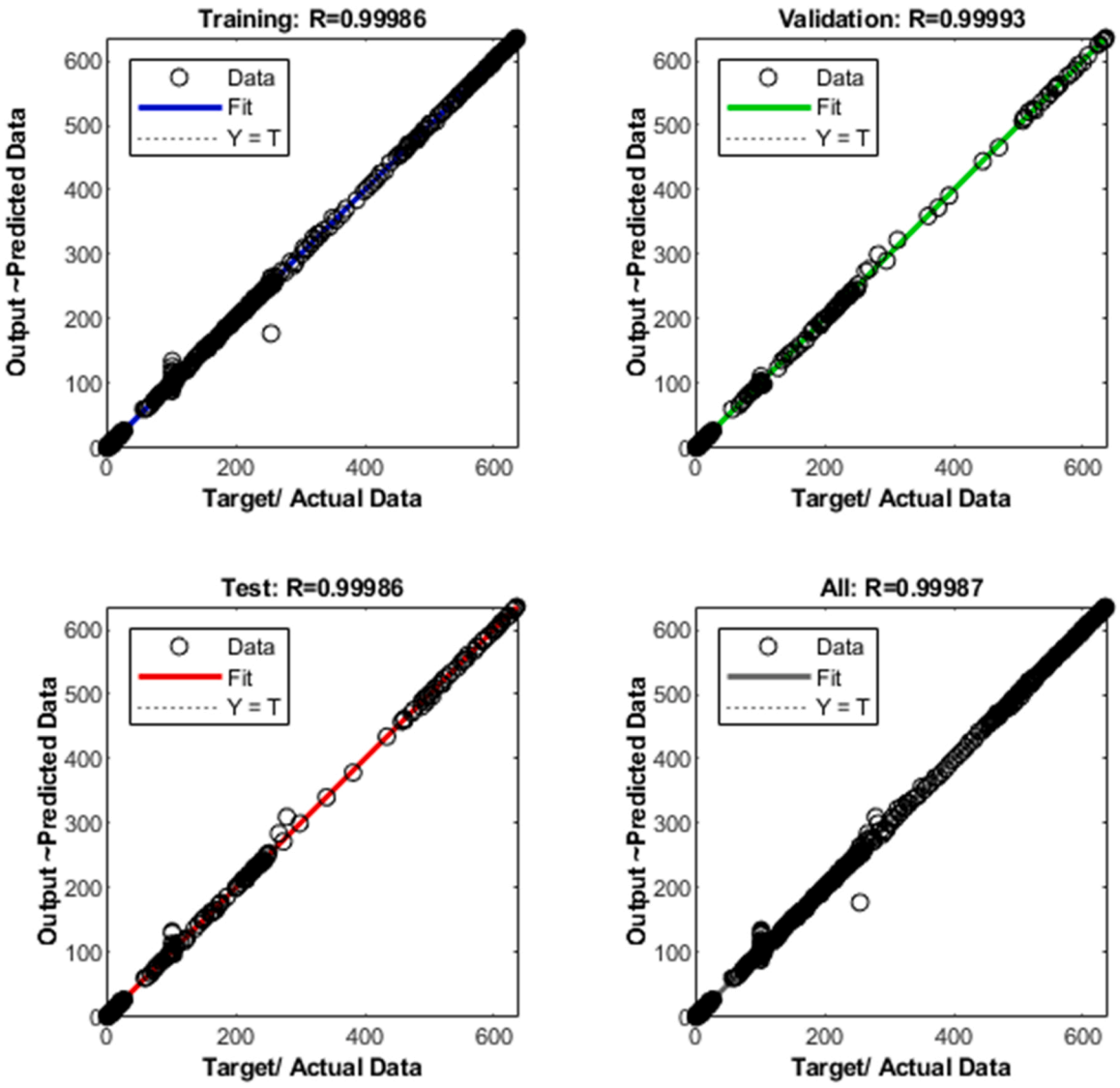

Fig. 12. The overall ANN scatterplot for testing, training, and validation portions.

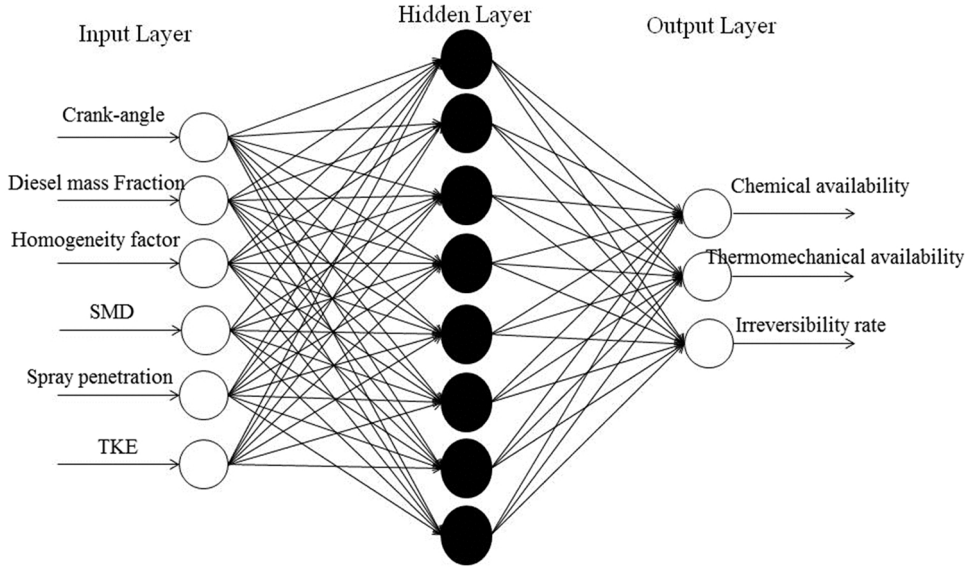

Fig. 13. The ANN block structure for the second case study: the injection angle grading.

Table 4
The impact assessment of injection angle with input and output data series.

Injection angle	Peak penetration (m)	HF (-)	Mean TKE (m^2/s^2)	Mean A_{tot} (J)	Mean dI/dθ (J/deg)
130 deg	0.03	0.703	15.68	191.09	17.48
140 deg	0.0294	0.69	15.09	165.05	14.88
150 deg	0.0277	0.671	14.23	154.3	12.98

during injection will have a lower chance of exergy content or energy accessibility for the final useful work conversion ratio. Hydrogen, on the other hand, features a tiny spray droplet with SMD = 2.55 μm and the highest HRR of HRR = 11.277 J/deg giving the most proportion of chemical and thermomechanical availability corresponding to 41% and 55%. This means that the fuel with small droplets generated during the breakup process can make a uniform air/fuel mixture. This premixed load to the engine (as featured by the modified homogeneity factor) can boost the pressure and temperature of the cylinder , where the availability terms are leveraged. Concerning irreversibility, diesel shows less exergy destruction potential (31%) whereas DME shows the most share of irreversibility (36%). The irreversibility of different fuels is close to each other.

The plots of Fig. 8 display the effect of main input variables on the output of thermomechanical availability in the engine. The results infer that by having a small spray droplet as the fuel jet breakup initiates, a better homogeneity factor (closer to 1) resulted, and this comes from better heat release and droplet evaporation by the oxidizer. On the other side, the heat-to-work ratio for the cases of better air-fuel mixing elevates due to the higher pressure of the in-cylinder chamber. The significance of mixing dynamics in better availability terms is emphasized in this study, where the fuel chemical potential can better be used and converted to heat and pressure. The goal is to prevent heat loss from the chamber walls and exhaust valve and make the pressure to move the piston, which gives higher availability of the system.

5.1.2. *ANN modeling results for the first case study-fuel type grading*

In this sub-category, the ANN is served to prognosticate the second law of thermodynamic, which govern the energy quality of the system. The main part of the present study deals with connecting the availability of energy and irreversibility with the factors of load preparation and premixed quality of fuels, injected spray structure, the generated heat of combustion, and gas species concentration. There have been no concrete mathematical equations in the exact form to link the aforesaid

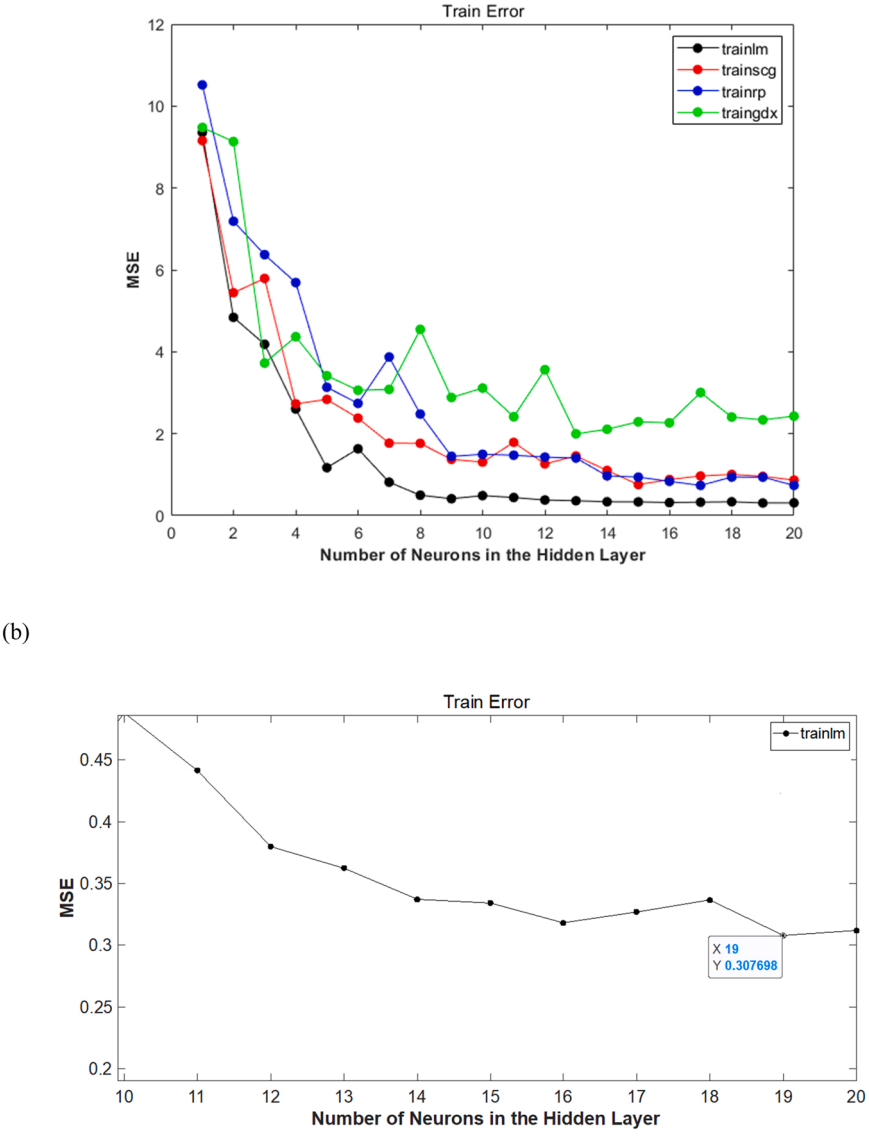

Fig. 14. (a) The MSE variation with the number of neuron layers for different training algorithms: the second case study, (b) magnified view of trainlm in the range of 10–20 neurons.

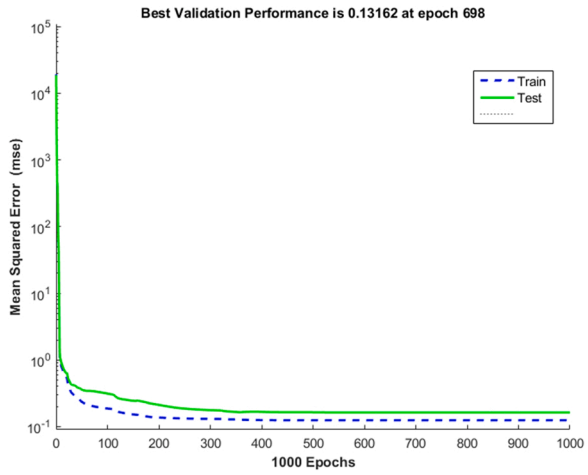

Fig. 15. The MSE variation versus epoch numbers to determine the best validation point for the testing and training dataset portions.

parameters, therefore this approach can be considered as black-box modeling in such intricate and stochastic physical phenomena as a combustion process.

The priority in ANN modeling is adopting the optimal configuration so that the efficiency and performance of the developed model in learning the pattern and predicting the accurate outputs can be increased. In this framework, a criterion for assessment of the accuracy and fidelity of the network must be established that here the actual responses and the deviations of the predicted response as the error is recognized and during each iteration, the model tries to minimize the respective error. Following, Fig. 9 displays the mean square error (MSE) with the increase of neurons in the hidden layer for different types of training methods thereby the best decision can be made on the optimal structure of the neural network. The transfer functions of trainlm, trainscg, trainrp, and traingdx are used in the range of 0–20 neurons. For all the cases, an increase of neurons caused the network error decline, however, trainlm and trainscg outperform in terms of the rapid gradient of error reduction compared to the other two algorithms. For the best architecture of network selection, trainlm in neuron number of $x = 20$ resulted in the least error of MSE = 0.3868. It seems like that in 10–20 neurons with the trainlm error variation is unchanged but in the magnified view of Fig. 8b, the minimum value of error that occurred in $x = 20$ is better illustrated.

As a result, the optimal neural network structure to achieve the precise modeling capability with the dataset as input and output is 7–20–3 with trainlm training algorithm. The MSE reduction trend for two subgroups of testing and training are shown in Fig. 10 and along with each epoch implementation, the error extent is reduced for the next step (the epochs are from 0 to 1000). Moreover, the optimal operative point from the cross-validation aspect happens at epoch number of 78 with the MSE corresponding to 3.3197.

The performance and precision of the ANN optimization with three statistical criteria for three output parameters are estimated and measured which are mentioned in Table 3. According to this table information, the highest network performance capacity (based on the coefficient of determination) for the training phase of the thermomechanical availability with $R^2 = 1$. It indicates that the success and adequate robustness of the ANN model is observed. Such a performance can only be achieved with a unique selection of input and output data and variables that have strong interconnection from a physical and chemical standpoint. Other than that, the neural network structure and training expertise depends on matching of datasets on the unity line. The other point of interest is the value of $R^2 = 0.9999$ for the chemical availability that is very close to the unity, representing a striking predictive capability of the neural network. Two other indices of performance assessments that are introduced here include RMSE and MAPE. The MAPE (as an error measuring indicator) has the least amount for thermomechanical availability ($MAPE_{Atm} = 0.002786$) and the highest amount pertains to irreversibility ($MAPE_{dI/d\theta} = 0.45033$). However, based on the RMSE error evaluation, the least error in ANN performance goes to chemical availability. Based on these two error estimation definitions, the MAPE can be a better standard of error recognition since it gives a normalized deviation of the predicted results from the actual corresponding responses thus better delineating the response deviations that are the source of errors.

The data points are distributed across the scatter plots of Fig. 11 where the vertical axis represents the results of ANN modeling, and the horizontal axis gives the actual values of the output results from the thermodynamic simulation of the combustion chamber, computed by the EES solver. The closer the data points mapped onto the unity line (represented in a red dotted line) the better the network performance in predicting the exergy of the combustion system. Interestingly, there is full conformity of the results in simulation and modeling for the thermodynamic availability while the irreversibility rate demonstrates the lowest agreement of the results between actual and network responses. The main reason for this can be traced to the oscillation and instability of the instantaneous irreversibility rate. The high degree of consistency in the results in the case of availability is the inclusion of all influencing input parameters from mechanical (physical) agents (i.e., injection and spray evolution) to heat transfer and species formation during the chemical reaction. It can be concluded that for the physical formulation of the exergy, the mixing dynamics of air-fuel must be included in the engine application.

The overall performance of the ANN model is shown in Fig. 12 as the

Table 5
A selected number of data from the input and outputs for the second case study.

CA (deg)	Diesel MF (-)	SMD (mm)	Penetration (m)	TKE (m^2/s^2)	HF (-)	A_{ch} (J)	A_{tm} (J)	dI/dθ (J/deg)
721	0.00433	1.43×10^{-2}	0.0269	14.775	0.02354	0.6554	72.25	7.98
726.8	0.05401	4.39×10^{-3}	0.02717	35.835	0.38797	7.051	193.3	10.57
734	0.08128	3.77×10^{-3}	0.02893	32.441	0.60502	12.48	255.1	6.319
744	0.08659	3.71×10^{-3}	0.02816	16.187	0.69723	16.9	261.2	0.4537
753	0.08618	3.65×10^{-3}	0.02831	11.854	0.70247	17.63	238	0.3541

Table 6
The ANN performance and precision in producing the output values for the second case study.

Output parameters	R^2		RMSE		MAPE	
	Test	Train	Test	Train	Test	Train
A_{ch}	0.9999	0.9998	0.07945	0.090862	0.029048	0.02996
A_{tm}	0.9999	0.9999	0.53716	0.52584	0.002197	0.002217
dI/dθ	0.9934	0.9961	0.36729	0.26402	0.183889	0.192855

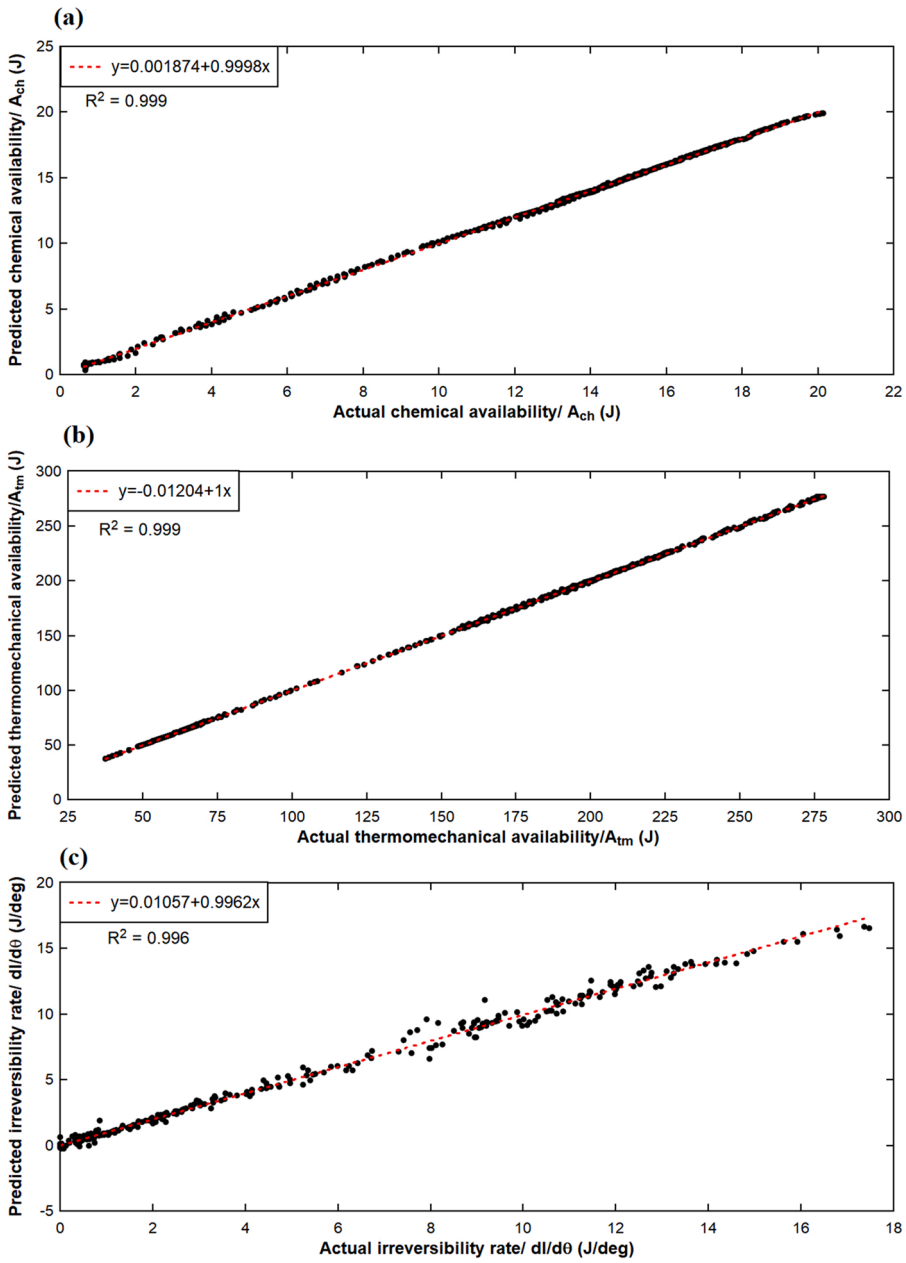

Fig. 16. The scatterplot for the ANN predictive results for (a) A_{ch}, (b) A_{tm}, (c) dI/dθ.

scatterplot for three phases of the classified data of testing, training, and validation. The correlation coefficient of the training mode is the highest that comes to R = 0.99993. The plot confirms the acceptability, robustness, and reliability of the training neural network with the proposed structure in producing the output exergetic responses. The present work is a combination of the CFD engine modeling, thermodynamic computation for the exergy and data-driven ANN.

5.2. The ANN application on energy-exergy interaction considering HF: the second case study- fuel injection angle grading*

This case study centers around the numerically generated data based on the different spray injection angle of diesel fuel, that consequently affects the mixing process and exergetic terms.

5.2.1. The network structure for the second sub-category

The undertaken process is exactly like the first case study but for the modeling goal, a different set of input data series such that 8748 data size is employed. The database is sorted according to injector injection angles of 130, 140, and 150 deg. The neural network structure is 6-x-3, and the number of neurons in the hidden layer will be determined based on the least MSE. The topological representation of the developed network for the second case is illustrated in Fig. 13 where the input parameter selection is also changed. At this time, the hydrodynamic spray characteristic of the spray penetration, turbulent kinetic energy (TKE), and diesel mass fraction are replaced by the major generated species concentrations, pressure, and HRR.

Table 4 summarized the information on the effect of an injection angle effect on the mixing index, turbulent kinetic energy, penetration and their correlation with the total availability, and irreversibility of the process taking place in the combustion chamber. Injection with 130 deg tilted angle allows for longer spray injection with a better atomization chance that results in higher HF* = 0.703. The mixing mechanics of fuel and air along with higher TKE for the case of injection with 130 deg results in higher energy available to be transformed to useful shaft work. The injection angle at the lower direction leads to spray-wall collision

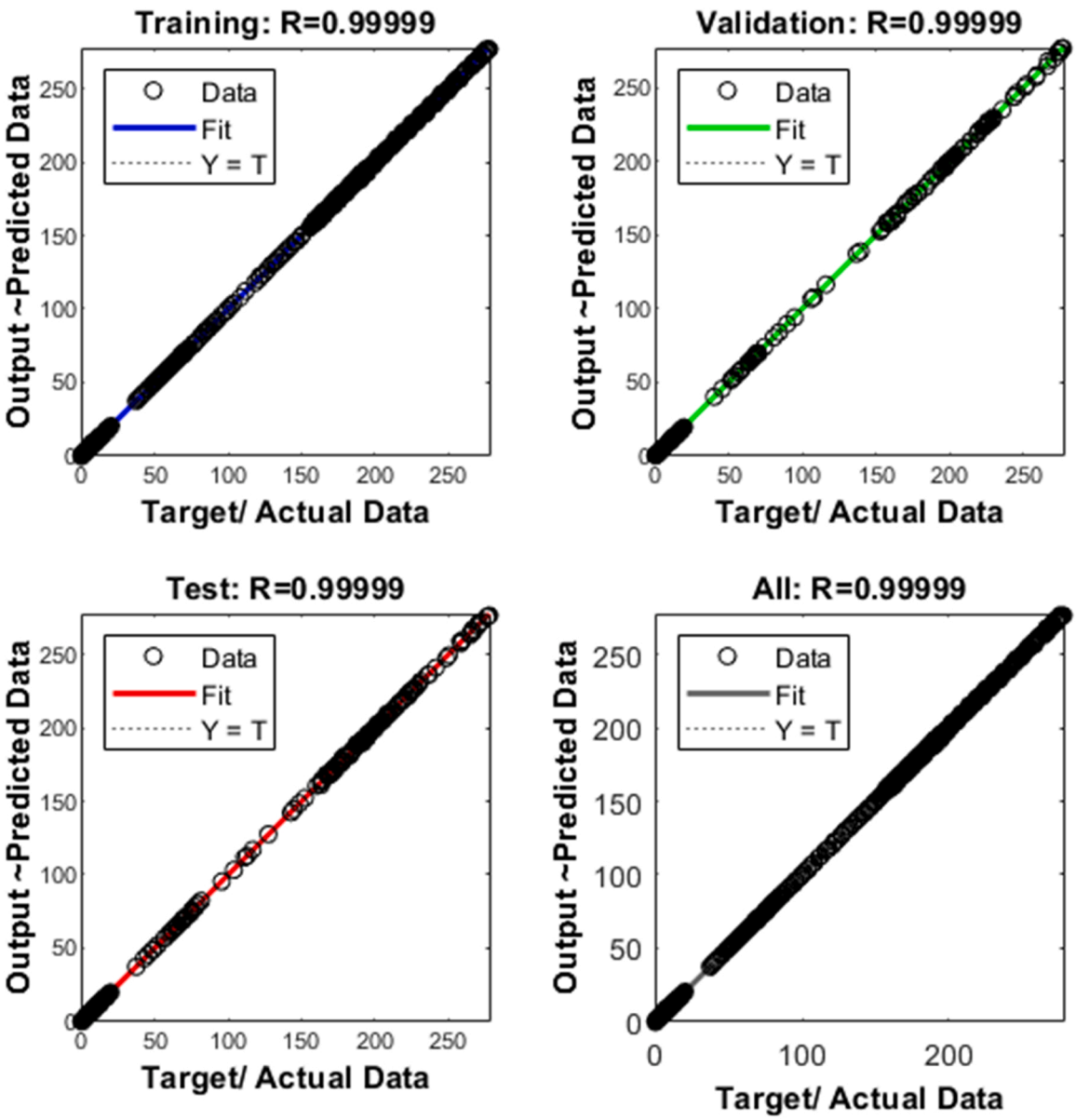

Fig. 17. The ANN performance in three phases of testing, training, and validation.

Table 7
The ANN comparison metrics between the study and recent literature.

Research item	Output parameters	Best R (R^2) network performance	Error analysis
Current study	Exergy/ irreversibility	$R^2 = 0.9999$	MAPE = 0.002197, RMSE = 0.09086
(Ma et al., 2022)	emissions	$R^2 = 0.9908$	MAPE = 0.0314
(Raptodimos and Lazakis, 2020)	Exhaust temperature	R = 0.9825	MAPE = 0.0104
(Castresana et al., 2022b)	Emission/ temperature/fuel consumption	R = 0.9968	MAPE = 0.0028
(Aghbashlo et al., 2016)	Exergy/ sustainability index	$R^2 = 0.9977$	RMSE = 0.13588

and reduces the air-fuel uniformity, thus an incomplete combustion process occurs. Therefore, the fuel chemical potential and heat production are wasted at 150 deg injection and the availability drops from 191.09 J to 154.3 J. Since the combustion at 150 deg is not fully happening, the process irreversibility is lower (around 25.7%) compared to 130 deg injection in the engine.

For the determination of x value, we use the top plot of Fig. 14 wherein the number of neurons for different training algorithms are varied. Again, trainlm algorithm proved better capability in error gradient reduction that is marked with a black line. The increase in a number of the hidden layer neurons in the standard interval (to avoid overfitting issues) leads to error reduction and the system performance enhancement. The enlarged picture of the trainlm algorithm is shown that a discernable least MSE at a neuron number of 19 corresponding to MSE = 0.3077.

Based on the obtained results, the optimal configuration of the neural network is 6–19–3 with trainlm for the second case study with the injection angle with different input parameters. In order to demonstrate the variation of the response errors versus, i.e. the number of iterations or epochs, Fig. 15 is given for two testing and training portions. The optimal validation performance is at 698th epoch with MSE = 0.13162.

A few randomly chosen data are sampled in the following Table 5. This table indicates that as the CA increases (or the time passes during

the engine functioning), the diesel fuel mass fraction or the amount of the injected fuel to the combustion chamber increases. Therefore, the fuel droplet diameter as a result of the breakup process decreases, then the spray penetration gradually increase, where the turbulence in the initial stage of injection has the maximum amount. It is seen that with the evolution of the process, the thermomechanical and chemical availabilities increase but the irreversibility decrease at the post-combustion stage.

5.2.2. The ANN application results on the second case study-grading based on the injection angle

For the assessment of the accuracy and reliability of the presented network, the statistical parameters are chosen to measure the degree of output response errors in the predictions. According to Table 6, the size of errors for all output parameters is minimal and the coefficient of performance is so close to unity indicating the excellent performance of the network due to an optimal selection of the network structure and the selected input parameters interconnection or influence on the thermo-mechanical index parameters. In this model (compared to the first case study), the model efficiency particularly in chemical exergy and irreversibility has upgraded significantly. That is to say, the determination coefficient for the test and training phases are improved from $R^2 = 0.978$ to $R^2 = 0.9934$ and $R^2 = 0.983$ to $R^2 = 0.9961$. The RMSE error deviation standard has the highest amount for mechanical availability, while the MAPE error criteria give the highest normalized error for irreversibility. This is mainly due to TKE consideration among the input variables that could cogently take into account the oscillatory nature of the instant irreversibility.

The 2D scatterplots around the fitting line, which is the index of correspondence of the actual and predicted values are depicted in Fig. 16. The data for the scatterplots are taken from the training phase for the output results. As seen, the mapping of data points around the fitting line for the availability terms is more than irreversibility which is also the case for the previous section.

It can be stated that the comprehensive effectual parameters on the exergy and the second law of thermodynamics will be selected that encompass the mechanical, combustive, heat transfer, chemical interaction, and species concentration parameters in two different categories of the first and the second case studies. The first case study is sorted for different alternative fuels of diesel, DME, and hydrogen while for the second case study the sorting of accessible data is implemented based on the fuel injection angle. In the first case study, the ideal performance of the network with $R^2 = 1$ is obtained and for the second case study, the efficiency of the system in predicting the irreversibility is improved. The overall neural network performance in three phases of testing, training, and validation is shown in Fig. 17 where the actual results of thermodynamic calculations are contrasted with the neural network modeling. The promising correlation coefficient of $R = 0.9999$ is an indication of the satisfactory performance of the neural network.

Table 7 shows the performance metrics, developed by an ANN and compared with the most relevant research metrics in the recent engine research studies. This study is having a larger data set and diverse input parameters. Having involved the computational parameter in a broad operational map, the introduced neural network model is able to predict the exergy output more efficiently in terms of the accuracy and performance as presented in Table 7.

6. Conclusion

A multi-fold research is conducted on the medium-speed marine diesel engine, which consists of CFD data, EES thermodynamic computation, and AI data processing to establish a connection among the energy, spray, and exergy parameters within the ANN framework. The main findings are:

- Thermomechanical availability increases with the increase of HF* that occurs along with a small SMD spray droplet size (SMD = 60 μm, HF* = 0.73 → $A_{tm,max}$ = 240 J).
- Hydrogen fuel with 55% of Atm and 41% of Ach gives the highest availability amount among the respective fuels. Although the irreversibility rate of all fuels is in the same range, DME has slightly more irreversibility (37%). The HRR of fuel has a direct correlation with availability while SMD has an inverse impact on the availability.
- The optimal ANN topology for the first case study (fuel type sorting) is 7–20-3 with trainlm algorithm, with which the corresponding mean error of MSE = 0.3868 is obtained. The neural network in this study is able to predict accurately the chemical exergy and thermo-mechanical exergy with respective $R^2 = 0.999$ and $R^2 = 1$ for the training portion of data. The MAPE index of results for A_{ch}, A_{tm}, and $dI/d\theta$ for the test portions are 0.061, 0.019, and 0.285.
- The 130 deg injection angle has a higher spray penetration length by making better mixture uniformity (HF* = 0.703) and TKE, as a result, higher total availability has been achieved. The availability and irreversibility quantities not only depend on the combustion process and pressure/temperature but also pertained to mixing pre-combustion dynamics.
- In the second case study, based on the RMSE error estimation criteria, the lowest amount goes to A_{ch} with 0.0908 while with MAPE error index A_{tm} demonstrates the lowest value as much as 0.0022. There is overall excellent performance of the output prediction with a machine learning approach for exergetic thermodynamic evaluation for a marine diesel engine application.
- For the second case study according to injection angle modeling and data sorting, the optimal configuration of the network is 6–19-3, wherein the model efficiency for the chemical and thermomechanical availability terms are considerably upgraded compared to the first case study. That is to say, for testing and training portions the predictive capacity are promoted from $R^2 = 0.978$ to $R^2 = 0.9934$ and from $R^2 = 0.983$ to $R^2 = 0.9961$ for the irreversibility rate.

The proposed research study on CFD data, exergy and HF computation, and then ANN application requires a considerable computational resources, however, the accuracy of the results can be guaranteed. To avoid this, the engineering device can be modeled with a 1D model in many situations. More detailed combustion parameters and gas species concentration will be considered in future works and that will increase the chemical exergy accuracy. Finally, the exergoenvironment and exergoeconomic parameters are of pivotal significance for promising renewable fuels and it is highly recommended to add these factors to the network's outputs , while keeping fuel price within the input array.

Declaration of Competing Interest

The authors declare that they have no known competing financial interests or personal relationships that could have appeared to influence the work reported in this paper.

References

Aghbashlo, M., Shamshirband, S., Tabatabaei, M., Yee, L., Larimi, Y.N., 2016. The use of ELM-WT (extreme learning machine with wavelet transform algorithm) to predict exergetic performance of a DI diesel engine running on diesel/biodiesel blends containing polymer waste. Energy 94, 443–456.

AVL FIRE version 2018, ICE Physics & Chemistry, Combustion, Emission, Spray, Wallfilm. AVL LIST GmbH, 2018.

Bejan, A., 2016. Advanced Engineering Thermodynamics. John Wiley & Sons.

Bui, K.Q., Perera, L.P., 2021. Advanced data analytics for ship performance monitoring under localized operational conditions. Ocean Eng. 235, 109392.

Cabrera, E., 2003. Heat flux correlation for spray cooling in the nucleate boiling regime. Exp. Heat Transf. 16 (1), 19–44.

Can, Ö., Baklacioglu, T., Özturk, E., Turan, O., 2022. Artificial neural networks modeling of combustion parameters for a diesel engine fueled with biodiesel fuel. Energy 247, 123473.

Castresana, J., Gabiña, G., Martin, L., Basterretxea, A., Uriondo, Z., 2022a. Marine diesel engine ANN modelling with multiple output for complete engine performance map. Fuel 319, 123873.
Castresana, J., Gabiña, G., Martin, L., Basterretxea, A., Uriondo, Z., 2022b. Marine diesel engine ANN modelling with multiple output for complete engine performance map. Fuel 319, 123873.
ChemBioPower, Inc, 2019. Emission Control Using Dimethyl Ether in Marine Applications. AZoCleantech, viewed 30 April 2022. ⟨https://www.azocleantech.com/article.aspx?ArticleID=714⟩.
Colin, O., Benkenida, A., 2004. The 3-zones extended coherent flame model (ECFM3Z) for computing premixed/diffusion combustion. Oil Gas Sci. Technol. 59 (6), 593–609.
Demirel, Y., 2007. Nonequilibrium Thermodynamics: Transport and Rate Processes in Physical, Chemical and Biological Systems. Elsevier.
Dincer, I., Rosen, M.A., 2012. Exergy: Energy, Environment and Sustainable Development. Newnes.
DNV, G.L., 2018. Maritime forecast to 2050. Energy Transition Outlook 2018.
Dukowicz, J.K., 1980. A particle-fluid numerical model for liquid sprays. J. Comput. Phys. 35 (2), 229–253.
Goulielmos, A.M., 2022. The initial 40 years of the EC Maritime Policy, Part I: 1957-1997: is EU-27 Maritime Industry "Fit for 55"? Mod. Econ. 13 (2), 159–185.
Hoang, A.T., Nižetić, S., Ong, H.C., Tarelko, W., Le, T.H., Chau, M.Q., Nguyen, X.P., 2021. A review on application of artificial neural network (ANN) for performance and emission characteristics of diesel engine fueled with biodiesel-based fuels. Sustain. Energy Technol. Assess. 47, 101416.
Hu, N., Zhou, P., Yang, J., 2017. Reducing emissions by optimising the fuel injector match with the combustion chamber geometry for a marine medium-speed diesel engine. Transp. Res. Part D Transp. Environ. 53, 1–16.
Huang, Z., Huang, J., Luo, J., Hu, D., Yin, Z., 2022. Performance enhancement and emission reduction of a diesel engine fueled with different biodiesel-diesel blending fuel based on the multi-parameter optimization theory. Fuel 314, 122753.
Işcan, B., 2020. ANN modeling for justification of thermodynamic analysis of experimental applications on combustion parameters of a diesel engine using diesel and safflower biodiesel fuels. Fuel 279, 118391.
Liu, J., Duru, O., Law, A.W.K., 2021. Assessment of atmospheric pollutant emissions with maritime energy strategies using bayesian simulations and time series forecasting. Environ. Pollut. 270, 116068.
Ma, C., Yao, C., Song, E.Z., Ding, S.L., 2022. Prediction and optimization of dual-fuel marine engine emissions and performance using combined ANN with PSO algorithms. Int. J. Engine Res. 23 (4), 560–576.
Maind, S.B., Wankar, P., 2014. Research paper on basic of artificial neural network. Int. J. Recent Innov. Trends Comput. Commun. 2 (1), 96–100.
Makoś, P., Słupek, E., Sobczak, J., Zabrocki, D., Hupka, J. and Rogala, A., 2019. Dimethyl ether (DME) as potential environmental friendly fuel. In E3S Web of Conferences, vol. 116, p. 00048. EDP Sciences.
Mobasheri, R., Peng, Z., 2013. CFD investigation into diesel fuel injection schemes with aid of Homogeneity Factor. Comput. Fluids 77, 12–23.
Moran, M.J., Shapiro, H.N., Boettner, D.D., Bailey, M.B., 2010. Fundamentals of Engineering Thermodynamics. John Wiley & Sons.
Nandha, K.P., Abraham, J., 2002. Dependence of fuel-air mixing characteristics on injection timing in an early-injection diesel engine (No. 2002–01-0944) (SAE Technical Paper).
Niu, X., Yang, C., Wang, H., Wang, Y., 2017. Investigation of ANN and SVM based on limited samples for performance and emissions prediction of a CRDI-assisted marine diesel engine. Appl. Therm. Eng. 111, 1353–1364.
Paul, A., Bhowmik, S., Panua, R., Debroy, D., 2018. Artificial neural network-based prediction of performances-exhaust emissions of diesohol piloted dual fuel diesel engine under varying compressed natural gas flowrates. J. Energy Resour. Technol. 140, 11.
Perera, L.P., Mo, B., 2016. Emission control based energy efficiency measures in ship operations. Appl. Ocean Res. 60, 29–46.
Perera, L.P., Mo, B., Soares, G., 2016. Machine intelligence for energy efficient ships: a big data solution. Marit. Eng. Technol. III, Guedes Soares St. (Eds.) 1, 143–150.
Popovac, M., Hanjalic, K., 2007. Compound wall treatment for RANS computation of complex turbulent flows and heat transfer. Flow Turbul. Combust. 78 (2), 177–202.
Rakopoulos, C.D., Michos, C.N., Giakoumis, E.G., 2008. Availability analysis of a syngas fueled spark ignition engine using a multi-zone combustion model. Energy 33 (9), 1378–1398.
Raptodimos, Y., Lazakis, I., 2018. Using artificial neural network-self-organising map for data clustering of marine engine condition monitoring applications. Ships Offshore Struct. 13 (6), 649–656.
Raptodimos, Y., Lazakis, I., 2020. Application of NARX neural network for predicting marine engine performance parameters. Ships Offshore Struct. 15 (4), 443–452.
Roh, H.G., Lee, C.S., 2017. Fuel properties and emission characteristics of dimethyl ether in a diesel engine. Locomotives and Rail Road Transportation. Springer, Singapore, pp. 113–128.
Roy, S., Banerjee, R., Bose, P.K., 2014. Performance and exhaust emissions prediction of a CRDI assisted single cylinder diesel engine coupled with EGR using artificial neural network. Appl. Energy 119, 330–340.
Shirvani, S., Shirvani, S., Jazayeri, S.A., Reitz, R., 2021. Optimization of the exergy efficiency, exergy destruction, and engine noise index in an engine with two direct injectors using NSGA-II and artificial neural network. Int. J. Engine Res. 14680874211057752.
Taghavifar, H., Mardani, A., Mohebbi, A., Taghavifar, H., 2014. Investigating the effect of combustion properties on the accumulated heat release of DI engines at rated EGR levels using the ANN approach. Fuel 137, 1–10.
Taghavifar, H., Taghavifar, H., Mardani, A., Mohebbi, A., Khalilarya, S., Jafarmadar, S., 2016. Appraisal of artificial neural networks to the emission analysis and prediction of CO_2, soot, and NOx of n-heptane fueled engine. J. Clean. Prod. 112, 1729–1739.
Taghavifar, H., Khalilarya, S., Jafarmadar, S., 2021. Computational and analytical measurement of air-fuel mixture uniformity and alternative fuels' ignition delay in ICEs. Renew. Energy 164, 767–776.
Terzi, R., 2018. Application of exergy analysis to energy systems. Appl. Exergy *109*.
Van Gerpen, J.H. and Shapiro, H.N., 1990. Second-law analysis of diesel engine combustion.
Versteeg, H.K., Malalasekera, W., 2007. An Introduction to Computational Fluid Dynamics: The Finite Volume Method. Pearson education.
Xu, X., Yan, X., Sheng, C., Yuan, C., Xu, D., Yang, J., 2017. A belief rule-based expert system for fault diagnosis of marine diesel engines. IEEE Trans. Syst. Man Cybern. Syst. 50 (2), 656–672.
Zeldovich, Y.A., Frank-Kamenetskii, D., Sadovnikov, P., 1947. Oxidation of Nitrogen in Combustion. Publishing House of the Acad of Sciences of USSR.
Zhou, J. and Xu, L., 2010, February. The fault diagnosis of marine engine cooling system based on artificial neural network (ANN). In 2010 The 2nd International Conference on Computer and Automation Engineering (ICCAE), IEEE, vol. 2, pp. 186–189.